Pre-clinical validation of in vitro engineered but cell-free human tissue grafts for skeletal regeneration

Alejandro Garcia Garcia[1,2,3], Sujeethkumar Prithiviraj[1,2,3], Deepak B. Raina[4], Tobias Schmidt[2,5,6], Aurelie Baudet-Quintino[1,2,3], Sara Gonzalez Anton[1,2,3], Laura Rabanal Cajal[1,2,3], Robin Kahn[2,5], Magnus Tägil[4], Paul Bourgine[1,2,3]

[1]Cell, Tissue & Organ Engineering Laboratory, Department of Clinical Sciences, Lund Stem Cell Centre, Lund University, Lund, Sweden

[2]Wallenberg Centre for Molecular Medicine, Lund University, Lund, Sweden

[3]Lund University Cancer Centre, Lund University, Lund, Sweden

[4]The Faculty of Medicine, Department of Clinical Sciences Lund, Orthopaedics, Lund, Sweden

[5]Division of Pediatrics, Department of Clinical Sciences Lund, Lund University, Lund, Sweden

[6]Division of Rheumatology, Department of Clinical Sciences Lund, Lund University, Lund, Sweden

Abstract

Tissue engineering strategies predominantly consist in the autologous generation of living substitutes capable of restoring damaged body parts. Persisting challenges with patient-specific approaches include an inconsistent performance, high costs and delayed graft availability. Towards developing a one-for-all solution, a more attractive paradigm lies in the exploitation of dedicated cell lines for the fabrication of human tissue grafts. Following decellularization, this new class of biomaterials relies on the sole extracellular matrix scaffold and embedded growth factors instructing endogenous repair. This conceptual approach was previously validated by manufacturing human cartilage using a custom mesenchymal line, exhibiting remarkable osteoinductive capacity following lyophilization. However, key criteria to ensure clinical translation include a proper decellularization as well as stringent assessment of both immunogenicity and regenerative performance. Here, we report the engineering and decellularization of human cartilage tissue with minimal matrix impairment. Ectopic evaluation in immunocompetent and immunocompromised animals reveal preserved osteoinductivity which correlates with M0 to M2 polarization from Day 7 post-implantation. By establishing in vitro human allogeneic co-culture models, we evidenced the immuno-regulatory properties of cell-free human cartilages, suppressing T cell activation upon mounting of an immune response by activated macrophages, monocytes and dendritic

cells. Last, the regenerative performance was stringently assessed in a competent rat orthotopic models whereby human cartilage grafts fully restored critical-sized femoral defects within six weeks, achieving native bone-like biomechanical properties by twelve weeks. Taken together, our study compiles safety and efficacy pre-requisites towards a first-in-human trial for engineered and decellularized human tissue grafts.

Introduction

Musculoskeletal traumas remain the first cause of disability affecting over 1.7 billion people worldwide[1]. Bone injuries and disorders account for a large fraction of this burden[2], creating a substantial demand for effective treatments that population aging only render more acute.

Tissue engineering has led to the development of a myriad of biomaterials and bioengineered substitutes shown to stimulate bone regeneration[3]. To enhance regenerative performance, a significant breakthrough involved incorporating developmental engineering principles into design strategies. This approach harnesses the natural process of endochondral ossification, where cartilage tissue is engineered to act as a transient template for bone formation[4]. To this end, Hypertrophic cartilage (HyC) can be generated in vitro by differentiating various cell sources, such as primary human mesenchymal stem/stromal cells (hMSCs), on scaffolding materials[5]. Upon implantation, the engineered HyC is gradually remodeled into mature bone matrix through the differentiation of chondrocytes into osteoblasts and the recruitment of endogenous osteoprogenitor cells[6].

Despite showing great promise in terms of graft integration and bone tissue restoration, key challenges inherent to autologous approaches remain to be overcome. These include donor site morbidity, limited availability, and variability, as well as inconsistencies in protocols for differentiating hMSCs into chondrocytes[7,8]. These factors add layers of complexity, making it difficult to standardize and optimize the process for consistent and effective clinical outcomes.

Limits of living strategies steered the development of an acellular alternative, whereby the regenerative process would solely be prime by the matrix and embedded factors from the graft. Our group has made significant contributions to this conceptual approach by

engineering cartilage tissues in vitro using the MSOD-B line as a source of immortalized hMSCs[9]. We demonstrated the scalable production of human cartilage that retains strong osteo-inductive properties even after lyophilization. This work established the foundation for manufacturing human tissue substitutes as off-the-shelf biomaterials capable of guiding and promoting bone repair.

While providing a strong proof-of-concept, the journey to clinical translation remains challenging due to the lack of complete decellularization and stringent performance assessments. The pre-clinical validation of cell-based but cell-free grafts is further complicated by the fact that this new class of biomaterials is yet to be fully defined by regulatory agencies[1,10]. Additionally, the suitability of standard pre-clinical models remains to be determined, as often falling short on replicating the complexity of the human immune system and physiological responses[11,12].

In this study, we aim at generating decellularized HyC and determine its immunogenicity and bone-repair capacity. Specifically, we propose evaluating the osteoinductive and immune recruitment using in immunodeficient and immunocompetent mouse models. We further design in vitro human immunogenicity assays, in which allogeneic monocytes, macrophages, and dendritic cells are analyzed for their ability to mount an immune response following exposure to decellularized HyC or non-decellularized HyC. Finally, HyC will be tested as a callus replacement biomaterial in a critical-sized femoral defect model.

By providing both safety and efficacy data, our work aims at prompting the clinical translation of human tissue grafts as engineered to instruct endogenous repair.

Results

Engineered human cartilage can be efficiently decellularized with minimal matrix impairment

We first seek to identify an optimal decellularization protocol offering both efficient DNA removal and preservation of tissue integrity. To this end, 12 protocols were evaluated including distinct detergent treatments (Triton X-100, SDC, and SDS), hypertonic and hypotonic baths, and DNase digestion time **(Supplementary Figure 1A)**. Human

hypertrophic cartilage pellets were first in vitro engineered as previously described[9] using the MSOD-B line (**Figure 1A**) and subsequently lyophilized. After exposure to various decellularization protocols, readouts consisted in measurements of total DNA and total of glycosaminoglycans (GAGs) for decellularization efficiency of matrix preservation respectively. Three protocols (Protocol 6, 9 and 12) were further evaluated based on their reduced impact on GAGs content and efficient DNA removal and were further evaluated by assessing BMP-2 and total collagen content (**Supplementary Figure 1B**), as well as histological analysis (**Supplementary Figure 1C**) of the resulting cartilage pellets. This allowed the identification of a protocol demonstrating robust decellularization (Protocol 12, **Supplementary Figure 1A**) from which resulting cartilage (D-Hyc) were further analyzed and compared to its non decellularized but lyophilized counterpart (L-HyC). SEM radiographs revealed an increase of surface porosity and exposure of the fibrillar matrix existing within the tissue, with no cells visible on the surface **(Figure 1B)**. While L-HyC samples displayed a homogenous cellular distribution, D-HyC showed no detectable fluorescence, confirming the absence of residual cells. Quantification of both DNA and GFP levels corroborated the successful decellularization, with the decellularized samples exhibiting negligible DNA levels (0.039µg/mg dry weight) as compared to L-HyC (13.4 µg/mg dry weight), a >99.7% reduction **(Figure1C)**. To quantify the impact on the cartilage ECM, we further assessed histologically the presence of GAGs, collagen type-2 and collagen type-X (**Figure 1D**). While D-HyC displayed presence of GAGs, a noticeable reduction was observed compared to L-HyC. This was further confirmed by a quantitative Blyscan assay, revealing a 12% loss in GAG content compared to non-decellularized controls **(Figure 1E)**. In contrast, analysis of other structural proteins, such as collagen, indicated preservation of collagen composition, as confirmed by the hydroxyproline assay **(Figure 1E)**, despite a differential organization of collagen II and collagen X networks evidenced by confocal microscopy. Interestingly, despite these morphological and compositional changes, the levels of BMP-2 embedded within the matrix remained unaffected (**Figure 1E)**.

Taken together, we here report the identification of an efficient decellularization protocol partially affecting the ECM architecture, particularly the depletion of GAGs.

<u>Decellularized human cartilage grafts fully remodeled into bone by ectopic priming of endochondral ossification in immunodeficient mice</u>

To assess whether the decellularization process affects the capacity of human-engineered cartilage grafts to undergo full endochondral ossification, we implanted lyophilized (L-HyC) and decellularized (D-HyC) grafts ectopically into immunodeficient mice (**Figure 2A)**. Early time-point analysis revealed that by day 7, the implanted cartilage began to be remodelled and colonized by host-recruited cells. By day 10, a thick peripheral layer of matrix was evident, showing intense Safranin-O (Saf O) staining and early signs of collagen deposition, as confirmed by Masson's trichrome staining (MT) (**Figure 2B**).

Following 6- and 12-weeks of implantation, histological and micro-CT analyses confirmed that both L-HyC and D-HyC grafts were fully remodelled into mature bone. Macroscopically, the red coloration of the explants indicated vascularization, while Safranin-O and Masson's trichrome staining demonstrated the replacement of cartilage with mature bone tissue, including marrow infiltration and the formation of a cortical bone layer with trabecular structures (**Figure 2B**). TRAP staining further revealed active osteoclast-mediated remodelling, consistent with mature bone turnover (**Figure 2C**).

Micro-CT radiographs confirmed bone mineralization (**Figure 2C**), and quantitative analysis of bone volume relative to tissue volume (BV/TV), bone volume (BV) or total volume (TV) revealed that at the 6-week mark, the decellularized group exhibited a thicker cortical bone layer than the control, as evidenced by higher BV/TV in the D-HyC samples (**Figure 2E**). However, by 12-weeks no significant differences between groups appeared. These results demonstrate that decellularization does not compromise the ability of engineered human cartilage grafts to support robust endochondral ossification in vivo.

To evaluate whether this dynamic would correlate in a fully functional immune system we implanted both L-HyC and D-HyC tissues into Black-6 mice (**Supplementary Figure 2A**). As in the immunodeficient model, we analyzed both short-term (3, 7, and 10 days) and long-term (6 and 12 weeks) time points. Histological analysis revealed higher levels of cellular infiltration and remodeling through the length of the tissue in both the L-HyC and D-HyC samples compared to the immunodeficient model (**Supplementary Figure 2B**), particularly by day 10. Furthermore, compared to the ID implantation model, MT staining revealed no early signs of collagen deposition at the periphery, highlighting the absence of the initial stages of bone formation that were evident in the ID setup.

At latest time points (6- and 12-weeks), none of the retrieved samples showed signs of complete bone remodeling. L-HyC samples remained largely unaltered, while D-HyC samples exhibited increased vascularization **(Supplementary Figure 2B).** Sample retrieval rates were approximately 80% for D-HyC at both time points, whereas only 40% and 20% of L-HyC samples were recovered at 6 and 12 weeks, respectively. Interestingly, despite the increased vascularization in D-HyC samples, both L-HyC and D-HyC tissues lacked significant mineralization, with L-HyC surrounded by fibrotic tissue and displaying minimal vascularization. Small areas of mineralization were detected in D-HyC samples and quantified via uCT, whereas mineralization in L-HyC was almost undetectable (**Supplementary Figure 2C**). TRAP staining confirmed the lack of bone remodeling, with no presence of osteoclastic activity in both conditions at 6 and 12 weeks (**Supplementary Figure 2C**).

These findings suggest that while D-HyC samples showed some vascularization and where less degraded, both groups failed to instruct bone in the immunocompetent model.

Decellularized human cartilage grafts exhibit lower immune recruitment but preserved pro-regenerative macrophage polarization capacity.

Given the successful bone formation observed in immunodeficient (ID) animals and the failure in immunocompetent (IC) animals, we performed an immune assessment following ectopic implantation of L-HyC and D-HyC grafts in ID (**Figure 3**) and IC (**Supplementary Figure 4**) mice, to establish a potential correlation between immune response and ectopic bone formation. Fully described phenotypes and markers of immune cells are found in **Supplementary Figure 3A**.

In ID, at day 7 we observed a greater number of recruited cells in the L-HyC group compared to D-HyC (**Figure 3A**). This disparity may result from the decellularization process, which has been shown to hinder cell colonization. By day 10, this difference was no longer evident. In terms of blood cell infiltration (CD45+), flow cytometry revealed that by day 3, both conditions exhibited comparable levels of CD45+cells, indicating similar early immune responses. However, by days 7 and 10 post-implantation, D-HyC grafts showed a significant reduction in total CD45+ immune cells compared to L-HyC ($p \leq 0.01$, $^{**}p \leq 0.0001$, determined by two-way ANOVA) (**Figure 3B**). To further investigate

whether the observed differences in total immune cell recruitment were associated with variations in immune cell composition, we analyzed the distinct populations over time (**Figure 3C**). Radar plots for immune cell populations, including macrophages (MΦ), natural killer cells (NKs), dendritic cells (DCs), T cells (Tcells), and B cells (Bcells), reveal a consistent pattern of immune cell response. Macrophages dominated the immune infiltration in both grafts and across all time points. On Day 3, macrophages were the most prevalent immune cells in both L-HyC and D-HyC groups, while the infiltration of other immune cell types remained minimal. By Day 7, the macrophage population remained the most abundant, though a slight increase in dendritic cells and B cells was observed. The trend persisted on Day 10, with macrophages still the most prominent immune cell type. Notably, differences in infiltration between L-HyC and D-HyC constructs were minimal, with only slight variations observed across all time points, as indicated by the closely aligned profiles for both constructs, with NKs showing the only significant difference at day 10, with higher recruitment in D-HyC compared to L-HyC. Detailed percentages of each immune cell subset are provided in **Supplementary Figure 3B**.

Given the predominant role of macrophages in both graft types, we further explored their polarization states (**Figure 3D**). We observed an expected trend associated with tissue healing: an initial unpolarized state, followed by a predominantly pro-inflammatory M1 profile at day 7, and a subsequent shift toward a pro-regenerative M2 phenotype by day 10. Importantly, macrophage polarization dynamics were similar between L-HyC and D-HyC grafts, indicating that despite differences in total immune cell infiltration, both graft types elicited comparable macrophage responses, with a shift toward a pro-regenerative environment over time.

Decellularized human cartilage grafts display a lower immune recruitment but fails at inducing macrophage polarization in immunocompetent animals.

Regarding IC mice, at early time points, total cell numbers in the control group remained consistently higher than in the decellularized group, though this difference was not statistically significant (**Supplementary Figure 4A**). Noteworthy, although no significant differences in total cell recruitment was observed between L-HyC and D-HyC grafts, more CD45+ cells were recruited in L-HyC grafts by day 10 (**Supplementary Figure 4B**). Immune infiltration patterns in IC mice showed macrophages as the key responders to

both L-HyC and D-HyC constructs, while other immune cell types remained less prominent during these early stages of remodeling (**Supplementary Figure 4C**). Unpolarized (M0) macrophages presented a marked increase over time. By Day 7, the percentage of M0 macrophages peaked in the L-HyC group**,** whereas the D-HyC group showed a more gradual increase, which continued to rise by Day 10. In contrast both M1 and M2, although spiking at Day 3, particularly in the D-HyC group, they showed a gradual decline over time (**Supplementary Figure 3D**). This trend suggests a dominance of unpolarized macrophages (M0) in the later stages of the early immune response in the immunocompetent animals. This lack of polarization is likely associated with the failure to form bone in IC animals.

Taken together, these results suggest that M2 macrophage polarization is essential for successful bone formation and that both L-HyC and D-HyC grafts exhibited comparable immune properties.

Decellularized engineered cartilage grafts promote distinct macrophage polarization with minimal M1 activation.

The disparity of macrophage polarization between ID and IC models underscores the need for human-based systems to accurately assess the immune response to these grafts. To address this, we developed an in vitro setup to evaluate macrophage polarization when exposed to L-HyC or D-HyC (**Figure 4A**). To maximize cell exposure to the graft material, both L-HyC and D-HyC were cryo-milled into fine powder prior to co-culture. Flow cytometry revealed lower M1 (CD80+, CD86+) and M2 (CD163+, CD206+) marker expression in macrophages cultured with D-HyC compared to L-HyC constructs (**Figure 4B**). To strengthen our assay, we utilized monocytes derived for up to 6-donors, overall keeping the same response within different donors (**Supplementary Figure 5A-B**).

As macrophages can function as antigen-presenting cells (APCs), either directly or through cytokine release, we next evaluated the T-cell response in co-cultures with macrophages exposed to powdered L-HyC and D-HyC grafts. T-cell proliferation analysis showed no significant differences in T-cell activation between the D-HyC and L-HyC groups, suggesting that both constructs elicited low adaptive immune responses in vitro (**Figure 4C**).

Human engineered cartilage grafts do not elicit a human adaptive immune response.

To further dig into the causes that lead to the low activation of T-cells, we then analyzed the potential role of tissue engineered cartilage to activate T-cells directly thought a co-culture with mononuclear cells (PBMCs) (**Figure 5C**) or dendritic cells (**Figure 5D**).

The first part of the experiment consisted of an in vitro culture assay involving a whole population of PBMCs directly treated with either L-HyC or D-HyC to assess their direct immunogenic potential through both cytokines' releases or direct cell-to-cell interaction (**Figure 5A**). To ensure the potential of this co-culture assay to promote T-cell activation, PHA was used as a positive control. Both CD4+ or CD8+ were analyzed after 5 days of co-culture, revealing little to no T-cell proliferation, similar between L-HyC and D-HyC groups (**Figure 5B**). As no T-cell proliferation was observed in the co-culture, we further investigated the differentiation profile of the T-cells to characterize their activation status. Flow cytometry was used to analyze the distribution of specific T-cell subtypes based on surface marker expression. Notably, L-HyC grafts exhibited a higher percentage of $CD4^{+}CD25^{+}$ T-cells, indicative of increased helper T-cell activation or regulatory T-cell presence. Conversely, D-HyC grafts showed a predominance of $CD8^{+}CD25^{+}$ T-cells, suggesting a shift towards cytotoxic T-cell activation. These findings highlight distinct activation profiles associated with each graft type, despite the absence of T-cell proliferation, suggesting differential immune modulatory effects (**Supplementary Figure 5C**). Pro-inflammatory cytokine release (IFN-γ and IL-6 and IL-10) was measured to further characterize immune activation. PBMCs co-cultured with D-HyC and L-HyC constructs produced similar levels of cytokines, confirming that both constructs exhibit low immunogenicity in vitro (**Figure 5C**).

To conclude, we also developed an assay involving the potential DC maturation in contact with the different L-HyC or D-HyC constructs (**Figure 5D**). Maturation markers (CD80, HLA-DR) were analyzed prior and after the assay **(Supplementary Figure 5D).** Both constructs induced low levels of DC maturation, comparable to baseline unstimulated negative control, further supporting the low immunogenic potential of decellularized cartilage grafts (**Figure 5E**).

Co-cultures with PBMCs or dendritic cells (DCs) further confirmed the low immunogenicity of both constructs, with comparable cytokine release and minimal DC maturation. These findings reinforce the immune-privileged nature of cartilage grafts.

Orthotopic immunocompetent rat critical-full sized femoral implantation of decellularized off-the-shelf MSOD-B cartilages confirms clinical potential.

To align with clinical requirements, we focused only on the D-HyC graft and implanted it into a critical-sized femoral defect in an immunocompetent rat model for 12-weeks (**Figure 6A**). To fulfill the 5mm defect, 3-pellets were implanted together (**Figure 6B**).

Micro-CT analysis revealed minimal bone formation in empty controls, with defects persisting across all time points, while D-HyC-treated groups showed progressive bone regeneration. At 4 weeks, D-HyC implants demonstrated significant bone deposition, which further increased at 6-and 12-weeks, achieving complete defect bridging by the final time point (**Figure 6C**). Explanted regenerated bone in the D-HyC group at 6-weeks indicated an ongoing process of remodeling mixing bone and cartilage areas within the defect (**Supplementary Figure 6**). Bone volume in the defect region was significantly higher in D-HyC groups compared to empty controls at all time points (****$p < 0.0001$; **Figure 6D**). Macroscopically, explanted femurs from D-HyC-treated rats exhibited full union in all samples (13/13), whereas none of the empty controls achieved union (0/6; **Figure 6E**). 3D reconstructions and cross-sectional views confirmed robust bone regeneration in the D-HyC group. Histological analysis with Masson Trichrome staining revealed organized cortical and trabecular bone structures in regenerated femurs, highlighting the capacity of D-HyC to support both structural and functional bone regeneration (**Figure 6F**).

Biomechanical testing further confirmed the functional restoration of the regenerated femurs. While D-HyC-treated defects exhibited lower ultimate peak force compared to empty controls (***$p < 0.001$), stiffness values were comparable (**Figure 6G**). These findings demonstrate that D-HyC grafts effectively regenerate bone in critical-sized defects, achieving both structural integrity and functional performance. These results highlight the regenerative potential of decellularized grafts, validating their use for bone repair in critical-sized defects, and supporting their potential for clinical application.

Discussion

In this study, we successfully generated decellularized HyC and demonstrated its immunoregulatory properties and bone-repair capacity through in vitro human immunogenicity assays and in vivo models. The resulting decellularized grafts exhibited remarkable osteoinductive properties in ID mice predicted by an early M2 polarization. Despite the absence of cellular debris, D-HyC could not prime ectopic bone formation in IC animals due to a lack of macrophage polarization detrimental to tissue remodelling. However, D-HyC supported robust bone regeneration in a critically sized femoral defect in immunocompetent rats, highlighting their promise as scalable, off-the-shelf solutions for clinical bone repair.

Despite the development of numerous graft types, only a limited number have reached clinical application. Current leading strategies predominantly rely on living constructs derived from various cell sources, demonstrating promising cartilage formation in vitro and successful bone formation in vivo[17–20]. However, these approaches face significant challenges, including graft-to-graft variability, inconsistent outcomes across implants, and the inherent risk of immunogenic responses with allogeneic grafts[21,22]. We, and others, have shown that devitalized cartilage templates can enhance bone regeneration [23,24]. However, the removal of immunogenic cell debris is essential for clinical translation but remains challenging due to the dense cartilage matrix[25]. In this study, we successfully established a decellularization protocol using optimized combinations of detergents (SDS), hypertonic and hypotonic buffers, and DNase treatment. This resulted in significant removal of cell-associated materials, with residual DNA levels below the recommended threshold (<50 ng/mg extracellular matrix)[26]. While decellularization led to a reduction in glycosaminoglycans (GAGs) and increased matrix porosity, these changes did not impair affect the grafts bone-forming capacity. To the best of our knowledge, this study is the first to demonstrate the full remodelling of a decellularized tissue into mature bone in both stringent ectopic and orthotopic models. These findings highlight the ability of the extracellular matrix, independent of living cells, to drive endochondral ossification and support robust bone regeneration.

While graft rejection was observed in the ectopic IC model, the implantation of D-HyC led to full regeneration at an orthotopic site. This highlights that beyond graft composition,

the local environment plays a pivotal role in regenerative decision-making. Despite several studies demonstrating endochondral ossification using hypertrophic cartilage in both ectopic and orthotopic models our graft outperforms pre-existing strategies in terms of both the speed and volume of new bone formation[6,19,21,35,36]. This validation of D-HyC in an orthotopic model significantly enhances its clinical translation potential.

Our study further demonstrates the importance of the initial immune response during bone formation[27], evidenced by compiled immune prints. In our study, macrophage polarization towards on M2 phenotype was shown to be predictive of a successful remodelling into bone. M2 macrophages have been described as active promoter of angiogenesis, tissue repair, and our results further support their involvement in bone formation[1,28–30]. In our study, the use of IC mice offers quantitative information of all recruited immune cells, towards assessing the immunogenic profile of our grafts. However, when exposed to an IC setting the remodelling process into bone could not be initiated. In fact, the removal of cellular debris did not significantly impact the early immune response observed, as both L-HyC and D-HyC fail to promote a healing response ultimately leading to an absence of bone formation. This indicates that despite DNA and cellular removal, interspecies variations in ECM proteins can still result in the immune rejection of cell-free tissues as observed in other studies with living cells[17,21,31].

Due to the inconsistency between models, we sought to evaluate both L-HyC and D-HyC in a humanized setup to analyze their performance and readability for clinical translation. Inspired by studies aiming at targeting immune response towards chondrocytes[32] or chondrogenically differentiated MSC[33,34], we developed three in vitro experiments to evaluated the capacity of L-HyC or D-HyC to induce an inflammatory or anti-inflammatory response and elicit acquired immunity when exposed to allogenic immune cells. Co-culture assays with macrophages demonstrated that decellularized grafts displayed reduced M1 (pro-inflammatory) and M2 (pro-regenerative) polarization compared to L-HyC. Both cartilaginous grafts suppressed T-cell activation and promoted an anti-inflammatory environment, essential for successful integration and regeneration as showed with the interaction of macrophages and T-cells and the direct stimulation of PBMCs, where in addition to low CD4 or CD8 T-cell activation, no inflammatory cytokines were found. When in contact with DCs, both L-HyC and D-HyC grafts demonstrated minimal DC activation, as evidenced by low levels of maturation markers (CD80 and HLA-

DR). These findings echo the results reported by Kiernan et al., who evaluated living allogeneic chondrogenically differentiated human mesenchymal stromal cells (hMSCs) and their interaction with PBMCs or DCs. The authors demonstrated that these living constructs did not induce T-cell-activation and failed to trigger DC maturation, supporting the hypothesis that the chondrogenic differentiation provides immunoprivileged status[33,34]. Our study extends previous findings by demonstrating that decellularized constructs, devoid of living cells, exhibit comparable immunomodulatory properties. The minimal DC maturation observed with D-HyC highlights the critical role of extracellular matrix (ECM) composition in modulating immune responses. This suggests that cartilage's immunoprivileged nature may stem primarily from its ECM, rich in glycosaminoglycans, collagens, and bioactive molecules, rather than its cellular components.

The development of decellularized tissue engineered grafts represents a promising approach for tissue regeneration, offering a scalable, off-the-shelf solution that bypasses the limitations of autologous and living grafts[13,14]. However, translating such biomaterials into clinical practice remains hindered by the lack of regulatory clarity, as their classification straddles the line between cell-based and acellular products. Recent regulatory advancements, such as FDA approval of an engineered acellular vessel[15], evidence regulatory path for acellular products although so far only applied from primary cells, not immortalized lines. Aside from categorization, the journey to clinical translation remains challenging, as current preclinical models—such as animal studies and simplified in vitro systems—fall short on replicating the complexity of the human immune system and physiological responses[12,16]. These limitations make it difficult to accurately assess how grafts will perform in humans, particularly regarding their safety, integration, and longevity within the body.

Taken together, our work demonstrates the possibility to engineer human cartilage tissue as bone graft substitute retaining potent bone formation capacity post-decellularization. It also highlights the limitations of existing in vitro and in vivo models to assess the immunogenicity and performance of human grafts deprived of a living fraction. Compiling robust pre-clinical safety and efficacy data will prompt the clinical testing of the cell-line derived but cell-free tissue graft.

Material and Methods

MSOD-B culture: MSOD-B cells (P21) are expanded in T175 flasks in complete medium consisting of alpha Minimum Essential Medium supplemented with 10% fetal bovine serum, 1% HEPES (1M), 1% Sodium pyruvate (100mM), 1% of Penicillin/Streptomycin/Glutamine solution and 5ng/ml of FGFb (all from Gibco Invitrogen, USA) under standard culture conditions until confluence (90%). Medium is replaced twice a week. Cells are seeded at a standard density of 3.400 cells/cm2.

MSOD-B seeding: MSOD-B cells (P23) are harvested and seeded on cylindrical collagen type I sponges (AviteneTM UltrafoamTM Collagen Sponge, Davol) of 6mm in diameter and 3mm in thick. Briefly, scaffolds are shaped with a 6mm biopsy punch (Kai Biomedical) and placed in a single well of a 12-well plate coated with 1% agarose to prevent cell adhesion. Per scaffold, 35µL of cell suspension containing 2M of cells are seeded at the surface and incubated 1h under standard culture conditions (cell culture media as seen before without FGFb). Then 2mL of chondrogenic medium is added to the well. This medium consisted of DMEM supplemented with 1% Insulin/Transferrin/Selenium, 1% Sodium pyruvate (100mM), 1% of Penicillin/Streptomycin/Glutamine (100X) solution (all from Gibco Invitrogen, USA), 0.47mg/mL linoleic acid (Sigma Aldrich, USA), 25mg/mL bovine serum albumin (Sigma Aldrich A2153-50G), 0,1mM ascorbic acid-2-phosphate, 10ng /ml TGFb3 and 10-7M dexamethasone. Chondrogenic medium is changed twice a week for a period of three weeks.

Lyophilization: After three weeks of hypertrophic differentiation, MSOD-B constructs are rinsed twice with PBS 7,2 (Gibco Invitrogen, USA). For lyophilization, cell constructs are then snap froze inside 15-ml tubes in liquid nitrogen for 5 minutes and then lyophilized at -80°C and 0.05mbar over night. Once freeze dried, the lyophilized cell constructs (L-HyC) are stored at 4°C for long term storage.

Decellularization: After lyophilization samples were immersed in a hypertonic solution (Tris-HCl 50mM, NaCl 1.5M, pH 7.6) for 10H at RT over continuous stirring (100rpm). After rinsing 3X with PBS at RT (30min each wash) each scaffold was immersed in a hypotonic solution (Tris-HCl 10mM, pH 8) ON at RT and over continuous stirring at 100rpm. Then samples were treated with SDS 0.5% in the hypotonic solution for 12H

(RT, 100rpm). Once treated with the detergent, samples were washed ON with the hypertonic solution (RT, 100rpm), subsequently washed three times with PBS as before for a total duration of 6H and treated with DNase I 50u/mL (Tris-HCl 10mM, pH. 7,6) and Aprotinin 10KIU/mL for 3H at 37°C under continuous stirring (100rpm) then washed 3X with PBS at RT (30min each wash). Once decellularized samples were lyophilized prior to implantation and quantitative analysis.

Powder formation: Only lyophilized (L-HyC) or decellularized and lyophilized (D-HyC) cartilages are then grinded with the CryoMill (RETSCH) in a 10 ml grinding jar of stainless steel with two 10 mm grinding balls. In order to ensure that the sample is pre-embrittled before grinding a pre-cooling time of 12 minutes is performed. Grinding is then performed for 4x 2 minutes at 25 hz and an intermediate cooling time of 30 seconds at 5Hz. Both powders are stored at 4°C for long term storage.

Biochemical analysis: After lyophilization, engineered human cartilage grafts are digested overnight at 56°C in 0.5 mL of a Proteinase K solution (Proteinase K, 1 mg/mL; pepstatin A, 10 µg/mL; 1 mM EDTA; 100 mM iodoacetamide; 50 mM Tris, all from Sigma) at pH 7.6. DNA content was evaluated fluorometrically using the CyQUANT NF Cell Proliferation Assay Kit (Thermo Fisher, USA), following the manufacturer's protocol (excitation at 485 nm, emission at 535 nm). Glycosaminoglycans (GAGs) content was analyzed by Glycosaminoglycan Assay Blyscan kit (Biocolor) following the manufacturer instruction. Total collagen was assessed by determining hydroxyproline content after acid hydrolysis (HCL 6N, 12H, 120°C), followed by a reaction with p-dimethylaminobenzaldehyde and chloramine T (Sigma-Aldrich, USA), applying a hydroxyproline-to-collagen ratio of 0.134. Both GAG and collagen contents are normalized to the dry weight of each sample. For BMP-2 protein content, human cartilage grafts were immersed in a RIPA buffer supplemented with protease inhibitor. Tissues are then lysed with a tissue homogenizer (TissueRuptor II, Qiagen) and total BMP-2 content within tissues was assessed using the human BMP-2 DuoSet ELISA (R&D Systems) according to the manufacturer's instructions.

Immunofluorescence staining: Samples were fixed in 4% paraformaldehyde (Thermo Scientific) at 4°C, for 24 h and decalcified with 10% EDTA solution (Sigma), pH 8 up to 2 weeks with gentle shaking, at 4°C. Embedding was performed using 4% low-melting agarose (Sigma) and 100 µm thick sections were cut using a 7000smz Vibratome

(Campden) with stainless steel or ceramic blades (Campden). All staining and washing steps were performed under gentle shaking. Sections were blocked and permeabilized with 0.5% Triton X-100 (Sigma) in PBS and 20% donkey serum (Jackson ImmunoResearch) for 1 h, at room temperature (RT). After blocking/permeabilization, sections were stained with primary antibodies at 4°C, overnight, and highly cross-absorbed secondary antibodies for 2-3 h, at RT with 3 times 20 min washes in between using 0.1% Triton X-100 in PBS and 2% donkey serum. Tissue sections were treated with Vector TrueView Autofluorescence Quenching Kit (Vector Laboratories) to remove unwanted fluorescence. Tissue sections were mounted with a Vectashield antifade mounting medium containing DAPI (Vector Laboratories, H1200). Samples were imaged with an LSM780 confocal microscope (Zeiss). We used the following primary antibodies: mouse anti-Collagen II (Invitrogen, MA137493) and rabbit anti-Collagen Type X (COL10) (abbexa, abx101469. The following secondary antibodies were employed: CF633 donkey anti-mouse (Sigma-Aldrich, SAB4600131) and CF568 donkey anti-rabbit (Biotium, 20098).

PBMCs preparation: Peripheral blood mononuclear cells (PBMCs) were isolated from heparinised blood using density gradient centrifugation (Lymphoprep, Axis-Shield) at 640g for 20 minutes with low break. The PBMCs were washed twice with PBS, counted, and prepared for subsequent assays. When required, monocytes were further isolated from PBMCs using CD14+ magnetic bead separation (Miltenyi) following the manufacturer's instructions, counted, and used in downstream assays. $CD4^+$ T-cells were isolated from the PBMC fraction using the EasySep™ $CD4^+$ T-cell isolation kit (Stemcell Technologies) as per the manufacturer's instructions.

Monocyte isolation and polarization in vitro: Monocytes were isolated from freshly isolated PBMCs, as described above, from healthy controls upon informed consent (n=6, median age 43, 50% female). Monocytes were next cultured for 5-days in 24-well plates (Falcon) at $0.5x10^6$cells/ml in complete alpha Minimum Essential Medium supplemented with 10% heat-inactivated fetal bovine serum, 1% HEPES (1M), 1% Sodium pyruvate (100mM), 1% of Penicillin/Streptomycin/Glutamine solution and 40ng/ml M-CSF. After 5-days, media was replaced and supplemented with 200µg/ml powdered engineered human cartilage grafts (L-HyC or D-HyC) without M-CSF and cultured for an extra two days.

Macrophage polarization analysis and preparation for T-cell proliferation: Forty-eight hour in vitro polarized monocytes were detached using ice-cold PBS/1mM EDTA and gentle pipetting. Next, they were washed with PBS, counted and resuspended in RPMI-1640 supplemented with 10% heat-inactivated fetal bovine serum, 1% of Penicillin/Streptomycin solution. $2.5x10^3$ cells were removed and used for the T-cell proliferation assay (see below). The remaining cells are washed with PBS and stained with anti-CD80, CD86 (clone FUN-1, BV650, BD), CD163 (clone: GHI/61, PE, BD) and CD206 (clone:19.2, APC, BD), all diluted 1:100, for 20min, RT. Finally, they were washed once more with PBS, counted and analysed by flow cytometry.

T-cell proliferation assay: T-cells were stained with 2μM CellTrace Violet (Invitrogen). A 96-well plate (Eppendorf) was coated with anti-CD3 (1:1000, Clone OKT3, Invitrogen) for 90min. The coating solution was removed prior to use. Wells without coating served as negative controls. In addition, anti-CD28 (clone CD28.2, Invitrogen, Thermo Fisher Scientific, 1:1000) coating was added in some wells as a positive control. Monocytes/macrophages from the in *vitro* polarization assay were counted (XN-350, Sysmex) and resuspended in RPMI-1640 supplemented with 10% foetal calf serum, 2mM L-glutamine and PenStrep. Next, monocytes/macrophages and T-cells at a 1:20 ratio (monocytes/macrophages: T-cells) were added to the coated plate in a total volume of 200μl. The cells were incubated for 72h, 37°C, at 5% CO_2. The cells were detached through gentle pipetting, centrifuged, and stained with anti-CD3 (clone UCHT1, alexa fluor 700, 1:200), anti-CD25 (clone M-A251, PerCP Cy5.51:200), anti-HLA-DR (clone G46-6, APC-H71:200) and anti-CTLA-4 (clone BNI3, PE, 1:50), all from BD, for 20min, RT. Finally, the cells were washed once with PBS and analysed using flow cytometry (CytoFLEX).

PBMCs analysis following powder activation: Previously lymphoprep isolated PBMCs were stained with 2μM CellTrace Violet (Invitrogen) for 20min. PBMCs were then resuspended in RPMI-1640 supplemented with 10% foetal calf serum, 2mM L-glutamine and PenStrep and culture at $0.5x10^6$ in 48-well plates (Falcon). Phytohemagglutinin-M (PHA-M, 10μg/ml, Roche) or anti-CD28 (clone CD28.2, Invitrogen, Thermo Fisher Scientific, 1:1000) coating were added in some wells as a positive control. PBMCs were then supplemented with 200μg/ml powdered engineered human cartilage grafts (L-HyC or D-HyC) and cultured for five days. At the end of the culture, media was collected for supplementary cytokines analysis and the cells were detached through gentle pipetting,

centrifuged, and stained with anti-CD3 (clone UCHT1, alexa fluor 700, 1:200), anti-CD4 (clone RPA-T4, alexa fluor 488, 1.5:100), anti-CD8 (clone RPA-T8, PeCy7, 1.5:100), anti-CD19 (clone SJ25-C1, BV786, 1:200), anti-CD25 (clone M-A251, PerCP Cy5.5, 1:200), anti-HLA-DR (clone G46-6, APC-Cy7,1:200), all from BD, for 20min, RT. Finally, the cells were washed once with PBS and analysed using flow cytometry (CytoFLEX).

IL-6, IL-10 and IFNg contenct within the supernatant was assessed using DuoSet ELISA (R&D systems) according to the manufacturer´s instructions.

Monocyte-derived dendritic cells (Mo-DCs) preparation and culture: Monocytes were isolated from freshly isolated PBMCs, as described above. Freshly isolated monocytes were seeded at $1x10^6$cells/ml in 24-well plate and cultured for five days following the ImmunoCult™ Dendritic Cell Culture Kit (STEMCELL) instructions. After five days, unmatured Mo-DCs were supplemented with 200µg/ml powdered engineered human cartilage grafts (L-HyC or D-HyC), ImmunoCult™ Dendritic Cell Maturation Supplement (STEMCELL) or left untreated for 48h, 37°C, at 5% CO_2. At the end of the culture, cells were detached using ice-cold PBS/1mM EDTA and gentle pipetting. Next, they were washed with PBS, counted and stained with anti-CD14 (clone 63D3, FITC, BioLegend, 1:100), anti-CD80 (clone 2D10, BV650, 1:100, BioLegend), anti-HLA-DR (Clone G46-6, PE-Cy7, BD, 1:100).

Ectopic implantation: *FoxN1* KO BALB/C (Nude mice) & C57BL/6J (wild type) mice of 6–8-week-old were obtained from Charles River Laboratories. All mouse experiments and animal care were performed in accordance with the Lund University Animal Ethical Committee (M15485–18) under the regulation of the Swedish board of agriculture following the 3R's principles. Mice were housed at a 12-hour light cycle in individually ventilated cages at a positive air pressure and constant temperature. Mice were fed with rodent chow and sterile water. Immune recruitment, tissue remodeling and bone formation efficiency of engineered human cartilage grafts is assessed by ectopic subcutaneous pouches in both ATHYM-Foxn1nu/nu mice and C57BL/6J mice, with a maximum of 6 implants per animal. For the surgical procedure, animals are anesthetized by inhalation using a mixture of oxygen (0,6mL min-1) and isoflurane (1.5-3vol%). After -3, -5 and-7-days or 6- and 12-weeks post implantation, samples were explanted and fixed in 4% formaldehyde solution (Solveco AB, Sweden) ON at 4°C prior to

microtomography and histological analysis (Safranin-O staining) or immediately digested for FACS analysis.

Critical-sized femoral defect implantation: Ten- to 12-week-old male Sprague Dawley rats (n=17) were purchased from JANVIER LABS (France). After 7 days of acclimation the rats were anesthetized using 3% isoflurane. Then, animals were placed on a 37°C warm heating pad in prone position. Once anesthetized, isoflurane was lowered to 2 to 2.5%, and buprenorphine (Temgesic, 30 µg/kg; Indivior Europe Ltd., Dublin, Ireland) was injected subcutaneously for analgesia. The right hind limb of the animal was shaved and carefully disinfected, and an incision was made along the skin and soft tissue to expose the right femur. After cleaning the femur laterally from soft tissue, a customized in house-developed four-hole internal fixation plate (Ø of 1.5-mm straight locking plate, PEEK) was held to the lateral aspect of the femur using forceps and a clamp. The plate was then screwed to the bone using two proximal and two distal screws (Ø of 1.5-mm locking screws, stainless steel; outer screws, 7 mm in length; inner screws, 6 mm in length; DePuy Synthes). After fixation, a 5-mm osteotomy was performed using two Gigli wires (0.44 mm; RISystem AG, Landquart, Switzerland) with the help of a custom-made, three-dimensional (3D) printed saw guide. The defect was then filled with three decellularized grafts. The grafts were push-fitted and not secured with any sutures. The wound was closed in a layered fashion using resorbable sutures (Vicryl 4-0, Ethicon, Somerville, USA) by closing the muscle first (continuous interlaced suture), followed by closing the skin (Donati suture). Animals started load bearing immediately after surgery. After 6 (n=2) or 12 weeks (n=15) animals were anesthetized by isoflurane inhalation (3%), followed by CO2 asphyxiation, and right-femur were harvested prior to subsequent micro-CT, mechanical and histological characterization.

All rat experiments and animal care were performed in accordance with the Lund University Animal Ethical Committee (18-08106/2018) under the regulation of the Swedish board of agriculture following the 3R's principles.

In vivo Micro-CT scanning: All rats were subjected to in vivo x-ray analysis at 4-6 weeks after surgery. Briefly, animals were anesthetized using isoflurane (3%) and placed in a right lateral decubitus position. Lower body was then scanned with a U-CT system (MILABS, Netherland) using a tungsten x-ray source at 50 kV and 0.21mA. A circular scan (360°) was recorded with an incremental step size of 0.250°. Volumes were reconstituted

at 30μm isotropic voxel size using MILABS software analysis. For bone volume analysis, the highly mineralized tissue volume was quantified using Seg3D (v2.2.1, NIH, NCRR, Science Computing and Imaging Institute (SCI), University of Utah, USA). For total volume analysis, each sample was meshed with Blender (v2.82a, Netherland) and analyzed with an in house developed script.

Ex vivo Micro-CT scanning: Subcutaneous (mice) and orthotopic (rat) implanted samples were fixed overnight with 10% formaldehyde before being subjected to ex-vivo micro-CT with a U-CT system (MILABS, Netherland) using a tungsten x-ray source at 50 kV and 0.21mA for subcutaneous retrieved samples and 65KV and 0.13mA for rat-femurs. Volumes were reconstituted at 10μm isotropic voxel size and analyzed for bone volume and total volume as described in the previous section.

Histological staining: L-HyC, D-HyC both in vitro or in vivo were washed in 1x PBS after formaldehyde fixation. Explanted in vivo tissues were decalcified with 10% EDTA (Sigma Aldrich, USA), pH 8.0, at 4°C for 2 weeks before paraffin-embedding. Tissues were progressively dehydrated using graded ethanol solutions (35%, 70%, 95%, and 99.5%; Solveco), with two 20-minute immersions per concentration. Following dehydration, the tissues were washed in a 1:1 mixture of 99.5% ethanol and xylene (Fisher Scientific) for 10 minutes, then treated with xylene alone for 20 minutes, twice. Subsequently, the tissues were embedded in paraffin at 56°C overnight and sectioned into 7–10 μm slices using a microtome. These sections were dried at 37°C overnight. To deparaffinize, the sections were rinsed twice in xylene for 7 minutes each, followed by a single 3-minute wash in 1:1 ethanol/xylene (99.5%). Rehydration was then performed using a graded ethanol series (99.5%, 95%, 70%, and 35%), with each step lasting 7 minutes and repeated twice.

Safranin-O staining: Sections Sections were stained with Mayer's hematoxylin solution (Sigma-Aldrich) for 10 minutes, followed by a rinse in distilled water to eliminate excess stain. Next, they were treated with 0.01% fast green solution (Fisher Scientific, USA) for 8 minutes, and any surplus dye was quickly removed by rinsing the sections in 1% acetic acid solution (Sigma Aldrich, USA) for 15 seconds. The slides were then stained with 0.1% safranin O solution (Fisher Scientific, USA) for 8 minutes. Dehydration and clearing were carried out by immersing the slides sequentially in 95% and 99.5% ethanol, followed by a 1:1 mixture of 99.5% ethanol and xylene. Finally, the sections were washed twice in

xylene for 2 minutes to remove any residual ethanol and mounted using PERTEX mounting medium (PERTEX, HistoLab).

Masson´s trichrome staining: Trichrome staining was conducted using the Trichrome Staining Kit (Sigma-Aldrich) in accordance with the manufacturer's protocol. Tissue sections were deparaffinized and rinsed as previously described. The sections were then placed in Bouin's solution (Sigma-Aldrich) either overnight at room temperature or for 15 minutes at 56°C. Following this, the slides were washed under running tap water and stained with Weigert's iron hematoxylin working solution (prepared by mixing equal volumes of solution A and B, EMD Millipore) for 5 minutes to visualize nuclei (stained black). After a wash step, the cytoplasm was stained red using Biebrich Scarlet-Acid Fuchsin for 5 minutes. The slides were then cleared by immersing them in a working phosphotungstic/phosphomolybdic acid solution (25 mL phosphotungstic acid, 25 mL phosphomolybdic acid, and 50 mL distilled water) for 5 minutes. Collagen fibers were stained blue by treating the slides with aniline blue solution for 5 minutes, followed by a clearing step in 1% acetic acid solution (prepared with glacial acetic acid, Fisher Scientific) for 2 minutes and a rinse under running deionized water. Finally, sections were dehydrated by sequential immersion in graded ethanol solutions (95% once, 100% twice) for 2 minutes each, followed by two 2-minute washes in xylene, and mounted with PERTEX mounting medium.

Flow cytometry: The experiment on immune cell recruitment was carried out using flow cytometry (FACS). Under sterile conditions, harvested subcutaneously implanted samples were carefully cleaned of the connective tissue. Three samples were pooled together for a single FACS sample and digested in an enzyme cocktail consisting of 300 U/mg collagenase type II (Sigma-Aldrich, U.S.A), 2 U/mg collagenase P (Sigma-Aldrich, U.S.A) and 2 mM $CaCl_2$ solution. The tissue digestion was carried out in a 12-well plate with 2 mL enzyme solution/well for 90 min in a humidified incubator at 37 ºC. Any tissue remnants were mechanically homogenized using a 10 mL pipette by repeatedly passing the tissue through the pipette tip. The enzymatic reaction was stopped by mixing an equal volume of cell culture medium containing 10% (v/v) fetal calf serum to the digest. Then the solution was passed through a 70 µM tissue strainer and collected in FACS tubes (BD, U.S.A). The cells from the digested tissues were centrifuged at 1500 rpm for 5 min, the supernatant was discarded, and the cells were resuspended in 1 mL FACS buffer (PBS 2%

v/v, 2 mM EDTA). 10 ul of sample was taken and mixed with equal volume of Tryphan blue and counted using Biorad TC20™ cell counting slides (Bio-Rad, Sweden). Cell suspension was re-spun to form a cell pellet, which was resuspended in 100 µL FACS buffer after which the respective primary antibodies for innate and adaptive immune system were added to the cell suspension and incubated at 4 ºC for 1 h. Antibody dilutions were added to compensation beads for setting up fluorescence compensation (UltraComp eBeads™ compensation beads, Thermofisher Scientific). At the end of incubation, cells were centrifuged, and the supernatant was discarded. Cell pellets was washed with 1 mL FACS buffer, centrifuged, and re-suspended in 350 µL FACS buffer containing nuclear stain DAPI (500 ng/ul). The cells were then analyzed on a BD LSRFortessa™ cell analyzer (BD, U.S.A).

Antibodies list: APC Fire CD11b (Rat IgG2b, κ) (Biolegend 101235), PE F4/80 (Rat IgG2a, κ) (Biolegend 123110), PECy7 CD11c (Armenian Hamster IgG) (Biolegend 117318), AF647 CD206 (Rat IgG2a, κ) (Biolegend 141712), BV650 NK1.1 (Biolegend 108736), PerCPCy5.5 CD45 (Rat IgG2b, κ) (Biolegend 147706), CD16/32 (Rat IgG2a, λ) (Biolegend 101302), APC Fire 750 CD8 (Rat IgG2b, κ) (Biolegend 344746), PE CD19 (Rat IgG2a, κ) (Biolegend 152408), PECy7 CD3 (Armenian Hamster IgG) (Biolegend 100220), AF647 CD4 (Rat IgG2b, κ) (Biolegend 100424).

Acknowledgements

Lund University Bioimaging Centre (LBIC), Lund University, is gratefully acknowledged for providing experimental resources. The Arbeitsgemeinschaft Osteosynthese (AO) Foundation (Development Incubator grant to P.E.B), the Knut and Alice Wallenberg Foundation, the Medical Faculty at Lund University and Region Skåne (grants to P.E.B), and the Swedish Research Council (Starting Grant No. 2019-01864 to P.E.B).

References

1. Khodabukus, A. *et al.* Translating musculoskeletal bioengineering into tissue regeneration therapies. *Sci. Transl. Med.* **14**, eabn9074 (2022).

2. Wu, A.-M. *et al.* Global, regional, and national burden of bone fractures in 204 countries and territories, 1990–2019: a systematic analysis from the Global Burden of Disease Study 2019. *Lancet Healthy Longev.* **2**, e580–e592 (2021).
3. Henkel, J. *et al.* Bone Regeneration Based on Tissue Engineering Conceptions — A 21st Century Perspective. *Bone Res.* **1**, 216–248 (2013).
4. Kronenberg, H. M. Developmental regulation of the growth plate. *Nature* **423**, 332–336 (2003).
5. Scotti, C. *et al.* Engineering of a functional bone organ through endochondral ossification. *Proc. Natl. Acad. Sci. U. S. A.* **110**, 3997–4002 (2013).
6. Bernhard, J. *et al.* Tissue-engineered hypertrophic chondrocyte grafts enhanced long bone repair. *Biomaterials* **139**, 202–212 (2017).
7. Bernhard, J. C. *et al.* Effects of Endochondral and Intramembranous Ossification Pathways on Bone Tissue Formation and Vascularization in Human Tissue-Engineered Grafts. *Cells* **11**, 3070 (2022).
8. Piñeiro-Ramil, M. *et al.* Usefulness of Mesenchymal Cell Lines for Bone and Cartilage Regeneration Research. *Int. J. Mol. Sci.* **20**, 6286 (2019).
9. Pigeot, S. *et al.* Manufacturing of Human Tissues as off-the-Shelf Grafts Programmed to Induce Regeneration. *Adv. Mater.* **33**, 2103737 (2021).
10. Dawson, J. I. & Oreffo, R. O. C. Bridging the regeneration gap: Stem cells, biomaterials and clinical translation in bone tissue engineering. *Arch. Biochem. Biophys.* **473**, 124–131 (2008).
11. Zeiter, S. *et al.* Evaluation of Preclinical Models for the Testing of Bone Tissue-Engineered Constructs. *Tissue Eng. Part C Methods* **26**, 107–117 (2020).
12. Petrus-Reurer, S. *et al.* Immunological considerations and challenges for regenerative cellular therapies. *Commun. Biol.* **4**, 1–16 (2021).
13. Hussey, G. S., Dziki, J. L. & Badylak, S. F. Extracellular matrix-based materials for regenerative medicine. *Nat. Rev. Mater.* **3**, 159–173 (2018).

14. Soltanmohammadi, F., Mahmoudi Gharehbaba, A., Alizadeh, E. & Javadzadeh, Y. Innovative approaches to tissue engineering: Utilizing decellularized extracellular matrix hydrogels for mesenchymal stem cell transport. *Int. J. Biol. Macromol.* **290**, 138893 (2025).

15. Commissioner, O. of the. FDA Approves First Acellular Tissue Engineered Vessel to Treat Vascular Trauma in Extremities. *FDA* https://www.fda.gov/news-events/press-announcements/fda-approves-first-acellular-tissue-engineered-vessel-treat-vascular-trauma-extremities (2024).

16. Adigbli, G. *et al.* Humanization of Immunodeficient Animals for the Modeling of Transplantation, Graft Versus Host Disease, and Regenerative Medicine. *Transplantation* **104**, 2290–2306 (2020).

17. Fahy, N. *et al.* Chondrogenically Primed Human Mesenchymal Stem Cells Persist and Undergo Early Stages of Endochondral Ossification in an Immunocompetent Xenogeneic Model. *Front. Immunol.* **12**, (2021).

18. Nilsson Hall, G. *et al.* Developmentally Engineered Callus Organoid Bioassemblies Exhibit Predictive In Vivo Long Bone Healing. *Adv. Sci.* **7**, 1902295 (2019).

19. Cunniffe, G. M. *et al.* Chondrogenically primed mesenchymal stem cell-seeded alginate hydrogels promote early bone formation in critically-sized defects. *Eur. Polym. J.* **72**, 464–472 (2015).

20. Bolander, J. *et al.* Healing of a Large Long-Bone Defect through Serum-Free In Vitro Priming of Human Periosteum-Derived Cells. *Stem Cell Rep.* **8**, 758–772 (2017).

21. Longoni, A. *et al.* Endochondral Bone Regeneration by Non-autologous Mesenchymal Stem Cells. *Front. Bioeng. Biotechnol.* **8**, (2020).

22. Kasravi, M. *et al.* Immunogenicity of decellularized extracellular matrix scaffolds: a bottleneck in tissue engineering and regenerative medicine. *Biomater. Res.* **27**, 10 (2023).

23. Bourgine, P. E. *et al.* Osteoinductivity of engineered cartilaginous templates devitalized by inducible apoptosis. *Proc. Natl. Acad. Sci. U. S. A.* **111**, 17426–17431 (2014).

24. Almeida, H. V. *et al.* Porous Scaffolds Derived from Devitalized Tissue Engineered Cartilaginous Matrix Support Chondrogenesis of Adult Stem Cells. *ACS Biomater. Sci. Eng.* **3**, 1075–1082 (2017).

25. Golebiowska, A. A., Intravaia, J. T., Sathe, V. M., Kumbar, S. G. & Nukavarapu, S. P. Decellularized extracellular matrix biomaterials for regenerative therapies: Advances, challenges and clinical prospects. *Bioact. Mater.* **32**, 98–123 (2024).

26. Crapo, P. M., Gilbert, T. W. & Badylak, S. F. An overview of tissue and whole organ decellularization processes. *Biomaterials* **32**, 3233–3243 (2011).

27. Burgan, J., Rahmati, M., Lee, M. & Saiz, A. M. Innate immune response to bone fracture healing. *Bone* **190**, 117327 (2025).

28. Zhang, D. *et al.* Research Progress of Macrophages in Bone Regeneration. *J. Tissue Eng. Regen. Med.* **2023**, 1512966 (2023).

29. Gou, M., Wang, H., Xie, H. & Song, H. Macrophages in guided bone regeneration: potential roles and future directions. *Front. Immunol.* **15**, (2024).

30. Zhu, Y. *et al.* Regulation of macrophage polarization through surface topography design to facilitate implant-to-bone osteointegration. *Sci. Adv.* **7**, eabf6654 (2021).

31. Maeda, A. *et al.* The Innate Cellular Immune Response in Xenotransplantation. *Front. Immunol.* **13**, 858604 (2022).

32. Pereira, R. C., Martinelli, D., Cancedda, R., Gentili, C. & Poggi, A. Human Articular Chondrocytes Regulate Immune Response by Affecting Directly T Cell Proliferation and Indirectly Inhibiting Monocyte Differentiation to Professional Antigen-Presenting Cells. *Front. Immunol.* **7**, 415 (2016).

33. Kiernan, C. H. *et al.* Allogeneic chondrogenically differentiated human mesenchymal stromal cells do not induce immunogenic responses from T lymphocytes in vitro. *Cytotherapy* **18**, 957–969 (2016).

34. Kiernan, C. H. *et al.* Allogeneic chondrogenically differentiated human bone marrow stromal cells do not induce dendritic cell maturation. *J. Tissue Eng. Regen. Med.* **12**, 1530–1540 (2018).

35. Pitacco, P., Sadowska, J. M., O'Brien, F. J. & Kelly, D. J. 3D bioprinting of cartilaginous templates for large bone defect healing. *Acta Biomater.* **156**, 61–74 (2023).

36. Herberg, S. *et al.* Scaffold-free human mesenchymal stem cell construct geometry regulates long bone regeneration. *Commun. Biol.* **4**, 1–16 (2021).

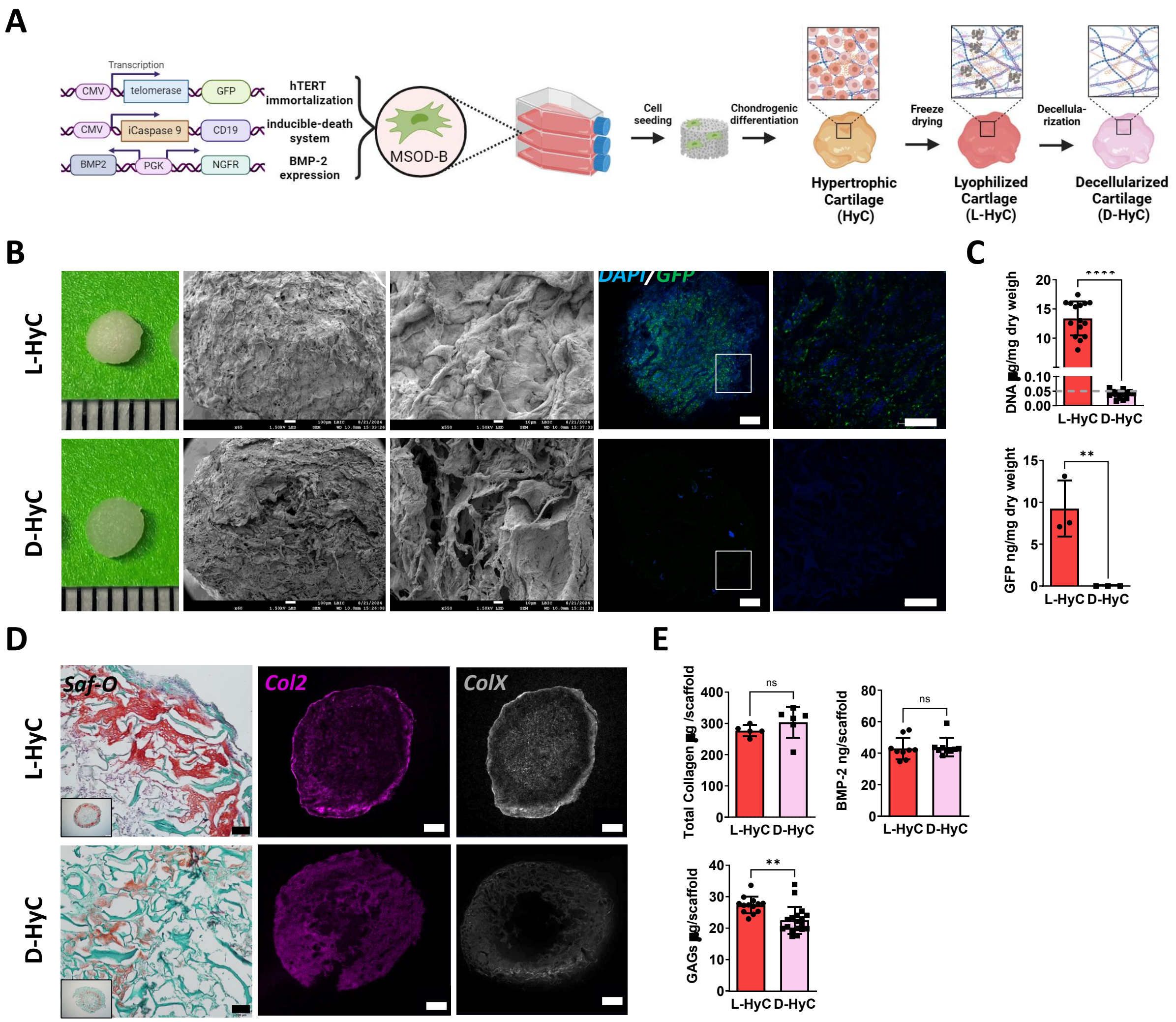

Figure 1: Engineered human cartilage can be efficiently decellularized with minimal matrix impairment. A. Experimental scheme for the generation of decellularized human cartilage grafts. **B.** From left to right: Macroscopic representation; scanning electron microscopy pictures of graft surfaces, Scale bar = 1mm and 100µm; and immunofluorescence confocal images of grafts stained for DAPI and GFP. **C.** From top to down quantification of total DNA (n=15) and GFP (n=3) remnants per mg dry weight of pellets. Dashed line represent the reported threshold for efficient decellularization (0.05 ugDNA/mg dry weight) established in the literature **D.** From left to right: Safranin-O staining and immunofluorescence images of human grafts stained for Col2 and ColX, Scale bar = 1mm. **E.** Quantification of GAGs (n=15), total collagen (n=6) and BMP-2 content (n=9) on decellularized and lyophilized grafts. Graphs represent mean +/- standard deviation (SD), $^{**}p \leq 0.01$, $^{***}p \leq 0.001$, determined by two-tailed unpaired *t*-test.

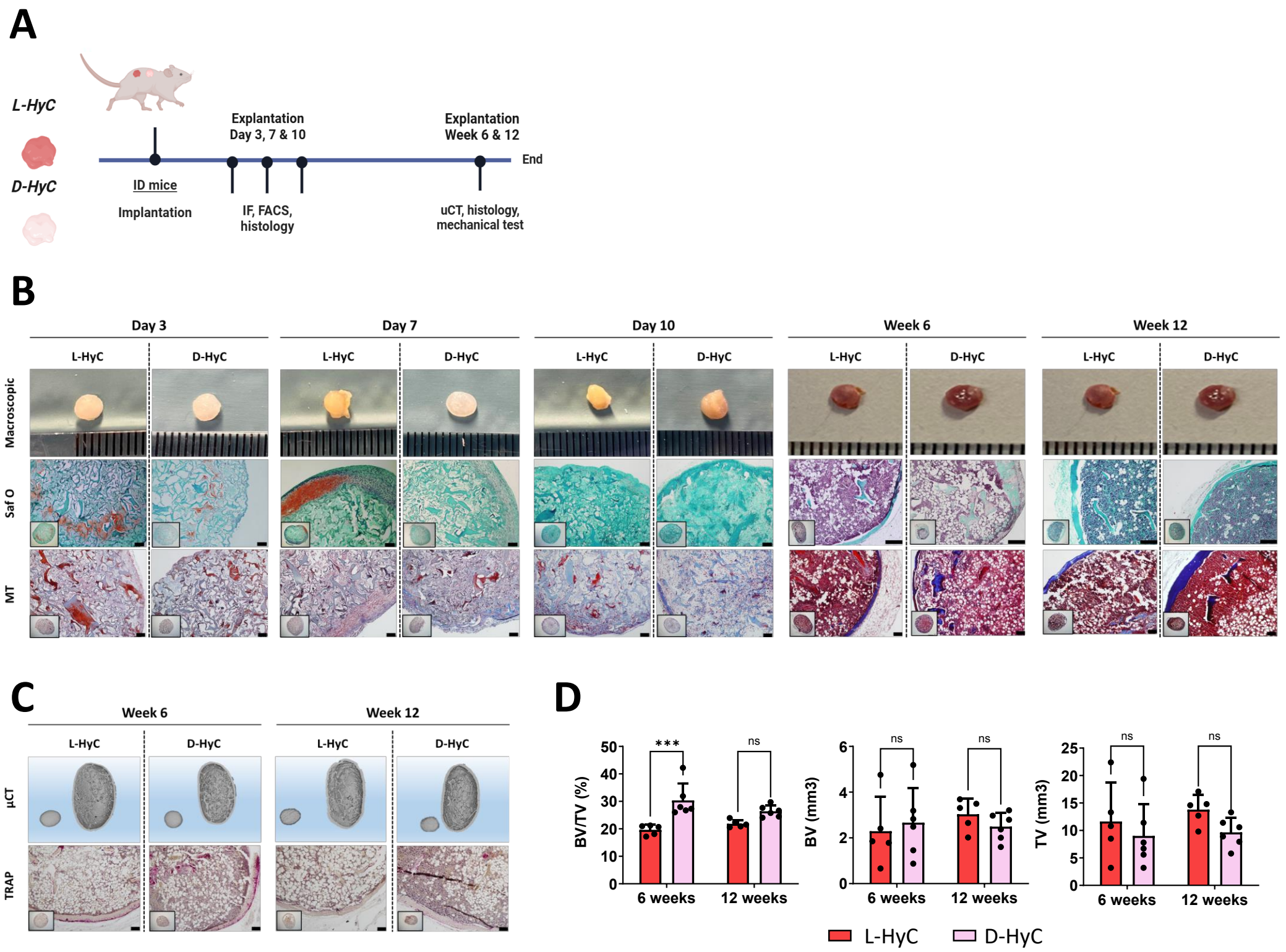

Figure 2: Decellularized human cartilage grafts fully remodeled into bone by ectopic priming of endochondral ossification in immunodeficient mice. A. Experimental scheme for the in vivo ectopic osteogenic assessment of L-HyC and D-HyC grafts. **B.** From top to down, representative macroscopic images (scale bar=1mm), histological images of Safranin-O and Masson Trichrome staining of explanted tissues (Scale bar =100µm). **C.** From top to down, representative µCT 3D reconstruction and TRAP staining of explanted tissues at -6 and -12-weeks (Scale bar =400µm). **D.** BV/TV (%), BV (mm^3) and TV (mm^3) of µCT performed over explanted bones at -6 and -12-week post-implantation (n≥5). The graphs represent mean + standard deviation (SD), *** $p \leq$, determined by Two-way ANOVA.

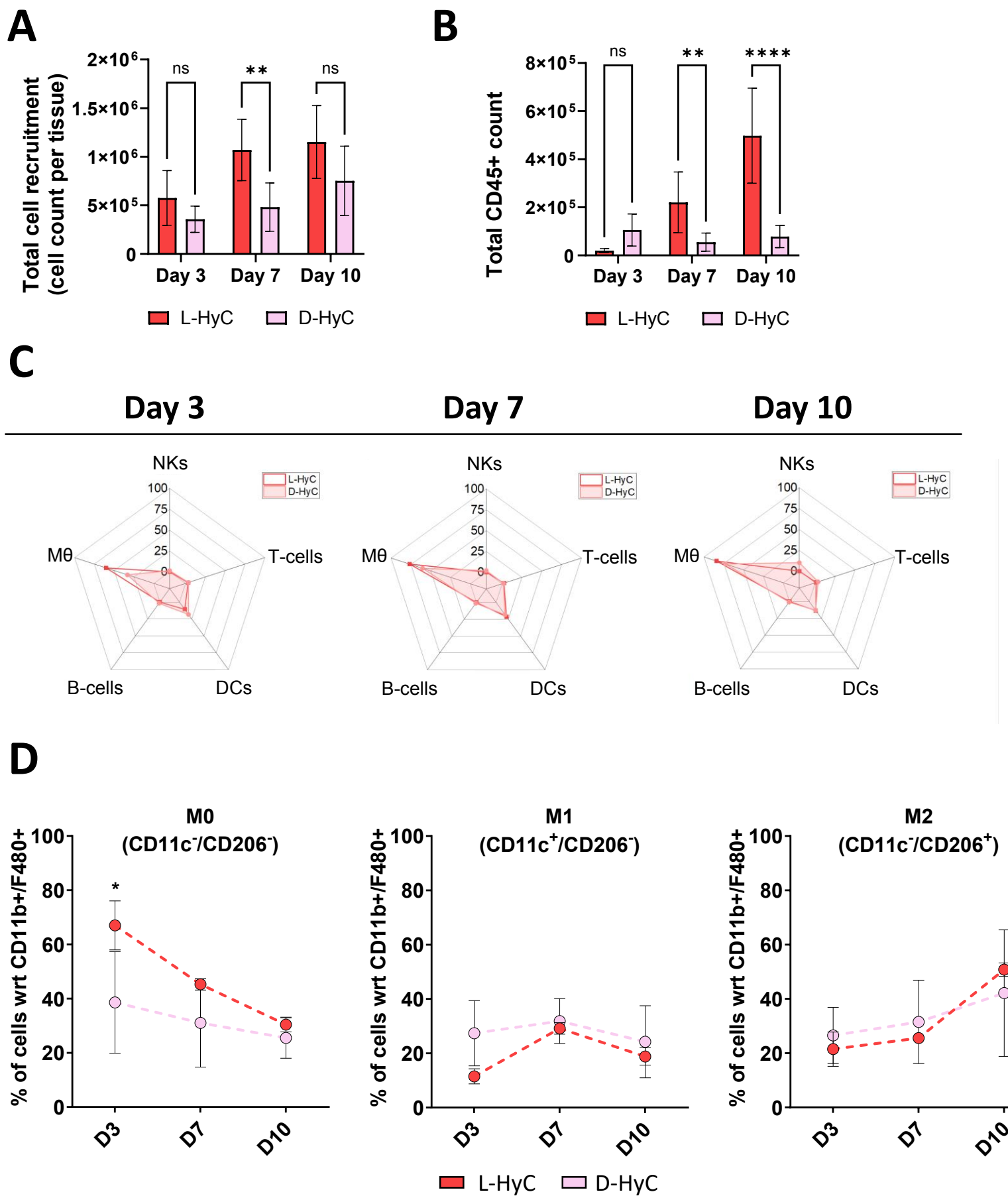

Figure 3: Decellularized human cartilage grafts exhibit lower immune recruitment but preserved pro-regenerative macrophage polarization capacity. A. Total cell number captured in explanted tissues after -3, -7-, and -10-days post-implantation. The graphs represent mean + standard deviation (SD), $^{**}p \leq 0.01$, determined by Two-way ANOVA. Total CD45+ cells captured by flow cytometry in explanted tissues after 3-, 7- and 10-days post-implantation **C.** From right to left, representative radar plots representing percentages of early time recruitment of B-cells, T-cells, Dendritic cells, Natural Killers and Macrophages captured in explanted tissues after -3, -7-, and -10-days respectively. **D.** Percentage of $CD11b^{+}$ and $F4\text{-}80^{+}$ macrophage subtypes in L-HyC and D-HyC grafts explanted at 3-, 7- and 10-days post-implantation analyzed by flow cytometry. Error bars: The graphs represent mean + standard deviation (SD), $^{*}p \leq 0.1$, determined by two-tailed unpaired *t*-test.

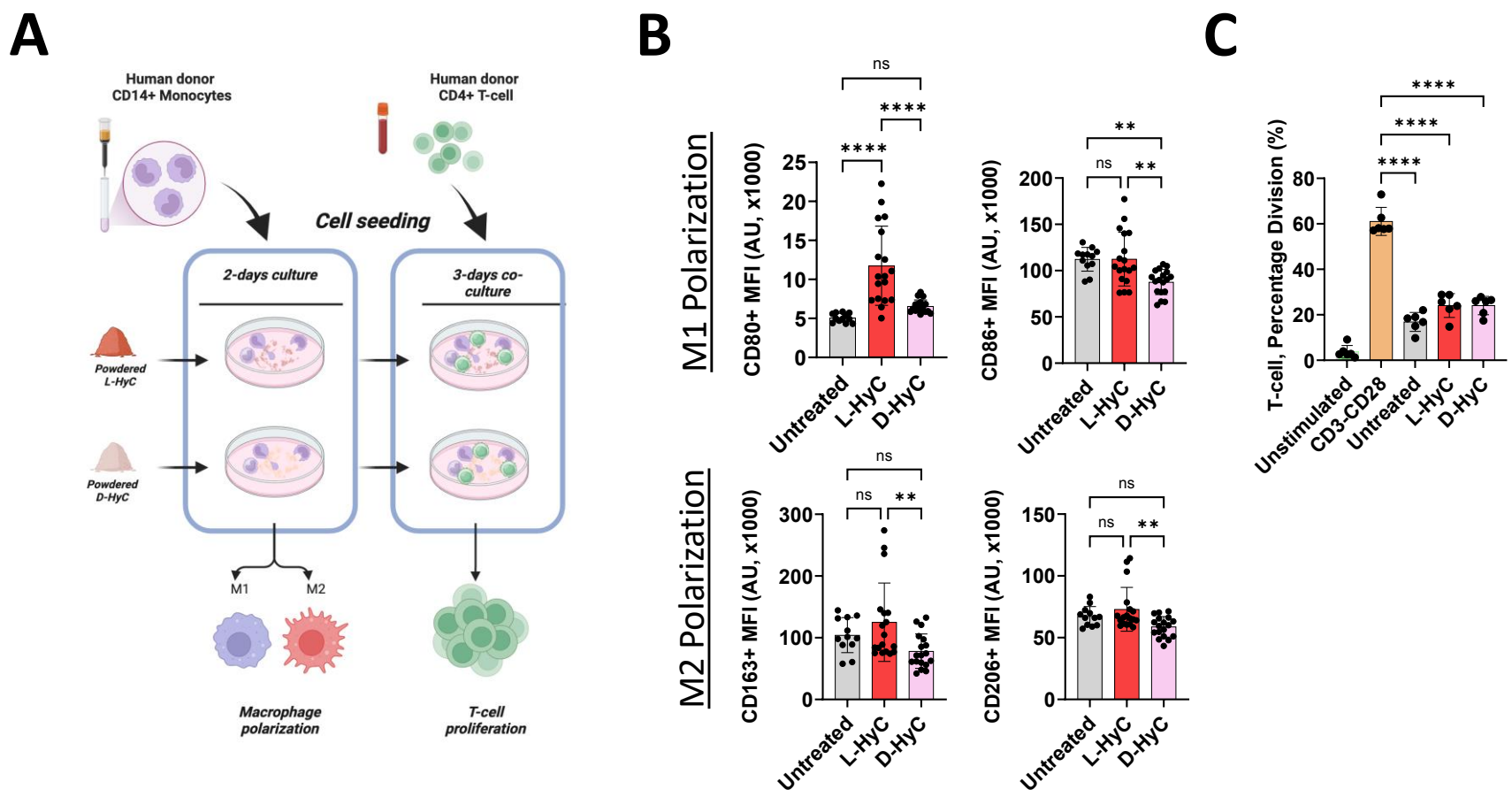

Figure 4: Decellularized engineered cartilage grafts promote distinct macrophage polarization with minimal M1 activation. A. Experimental scheme of the direct effect of powdered L-HyC and D-HyC on macrophage polarization and indirect T-cell activation potential. **B.** From top to down, total CD80+ and CD86+ MFI indicating M1 polarization; and total CD163+ and CD206+ MFI indicating M2 polarization, after 5-days co-culture with either L-HyC or D-HyC powdered cartilages. The graphs represent mean + standard deviation (SD), *$p \leq 0.1$ **$p \leq 0.01$, *** $p \leq 0.001$ ****$p \leq 0.0001$, determined by Ordinary one-way ANOVA **C.** CD3+ percentage division assessed by FACS after co-culture of $5x10^4$ CD3+ cells with $2.5x10^3$ macrophages co-cultured with either L-HyC or D-HyC powdered cartilages. The graphs represent mean + standard deviation (SD), ****$p \leq 0.0001$, determined by Ordinary one-way ANOVA

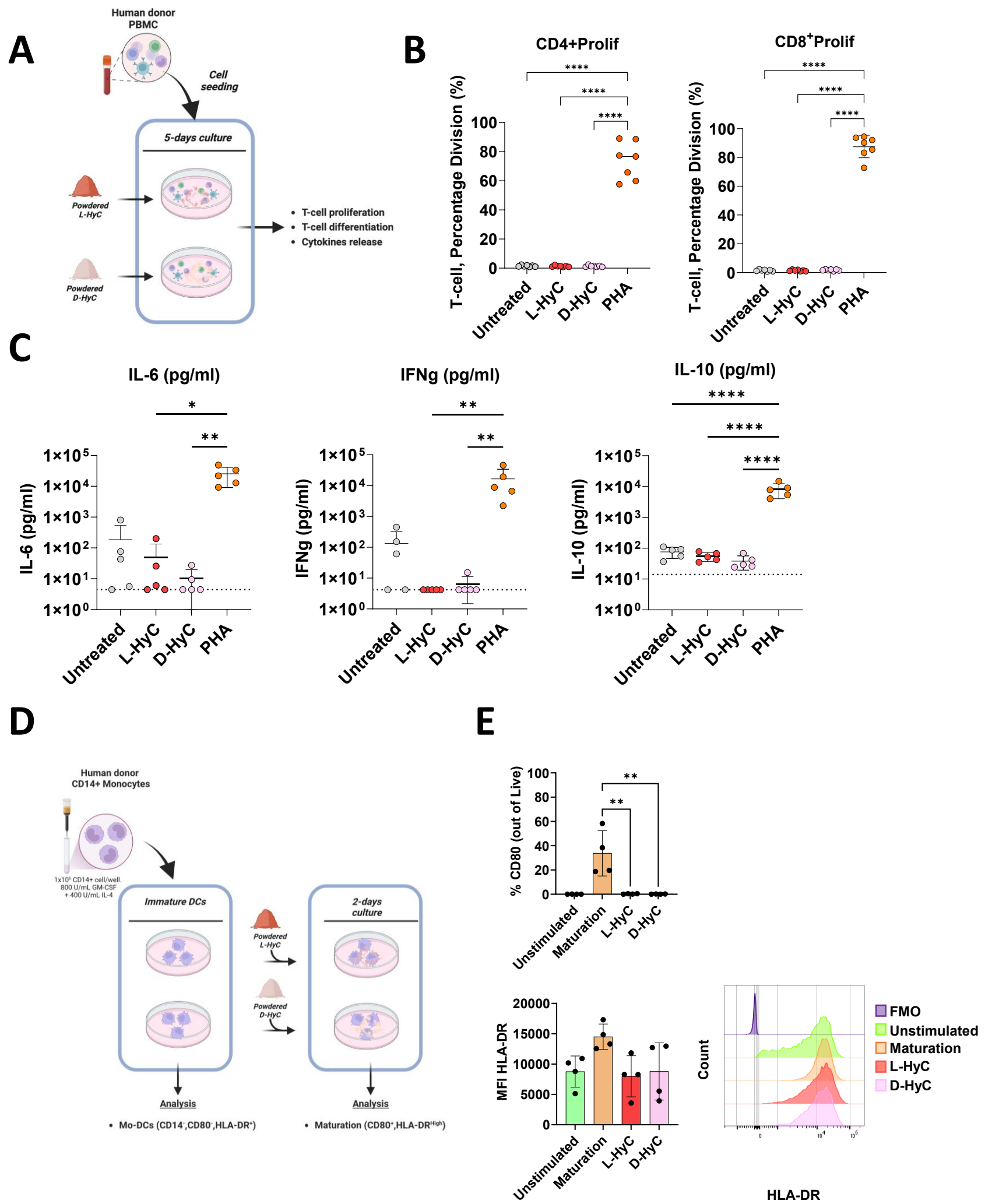

Figure 5: Human engineered cartilage grafts do not elicit a human adaptive immune response. A. Experimental scheme of the direct effect of powdered L-HyC and D-HyC on T-cell activation when directly co-cultured with PBMCs for 5 days **B.** From right to left, percentage of activated CD3+CD4+ and CD3+CD8+ T-cells. The graphs represent mean + standard deviation (SD), ****$p \leq 0.0001$, determined by Ordinary one-way ANOVA **C.** Pro-inflammatory cytokines released by PBMCs after 5 days co-culture with either L-HyC or D-HyC powdered cartilages. The graphs represent mean + standard deviation (SD), ****$p \leq 0.0001$, determined by Ordinary one-way ANOVA **D.** Experimental scheme of the assessment of dendritic cell maturation when cultured with either L-HyC or D-HyC powdered cartilages or maturation media in combination with powdered cartilages for 48H **E.** From up to down, percentage of CD80+ and total HLA-DR+ MFI of dendritic cells dendritic cells when exposed with either L-HyC, D-HyC powdered cartilages or maturation media in combination with powdered cartilages for 48H. The graphs represent mean + standard deviation (SD), **$p \leq 0.01$, determined by Ordinary one-way ANOVA.

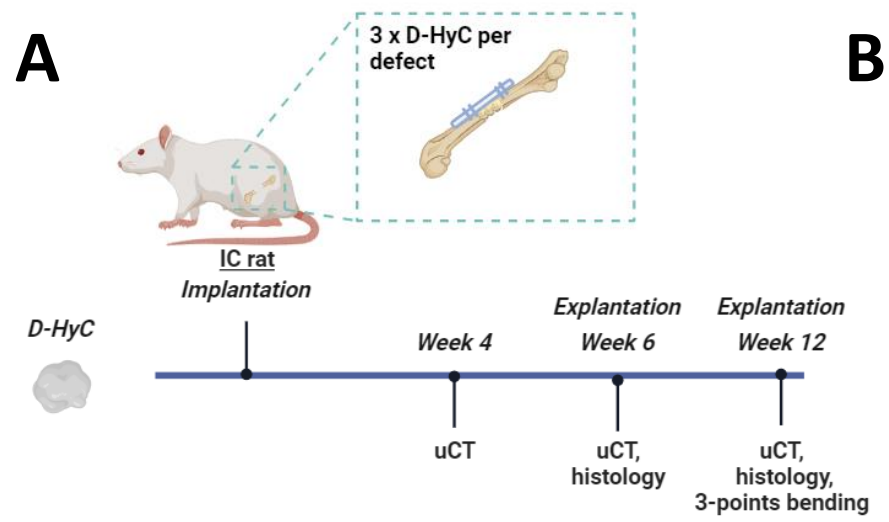
A
3 x D-HyC per defect
IC rat
Implantation
D-HyC
Week 4
Explantation Week 6
Explantation Week 12
uCT
uCT, histology
uCT, histology, 3-points bending

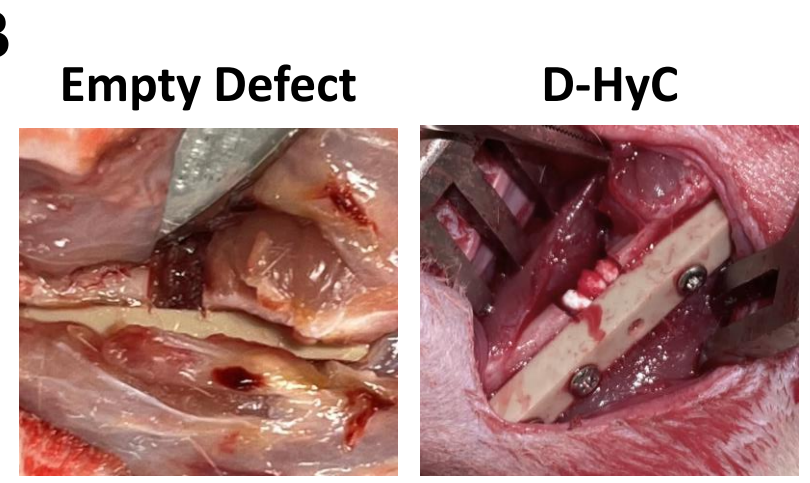
B
Empty Defect
D-HyC

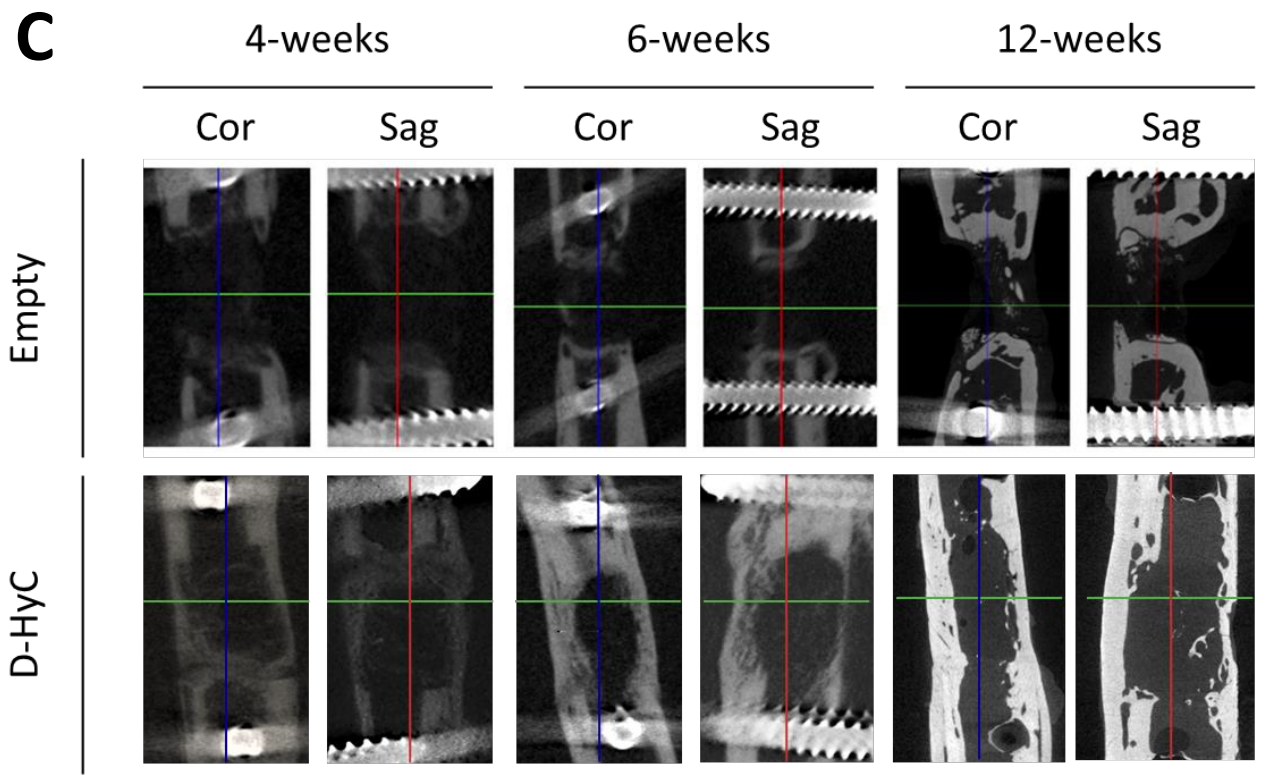
C
4-weeks
6-weeks
12-weeks
Cor
Sag
Cor
Sag
Cor
Sag
Empty
D-HyC

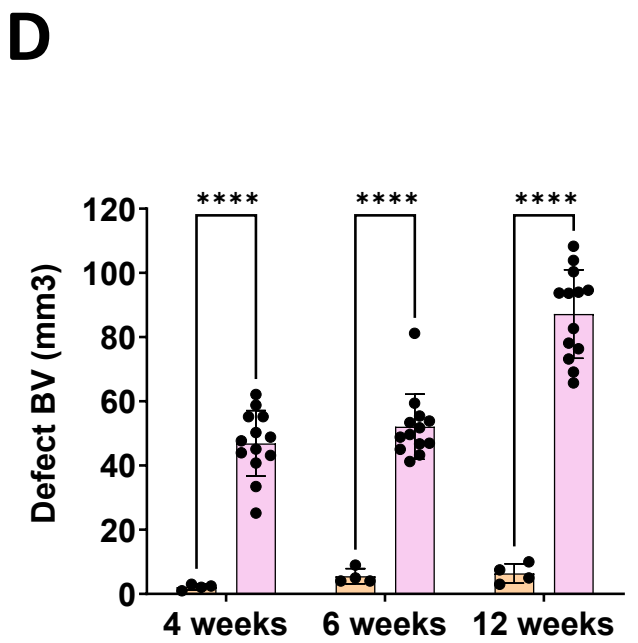
D
Defect BV (mm3)
120
100
80
60
40
20
0
****
****
****
4 weeks
6 weeks
12 weeks

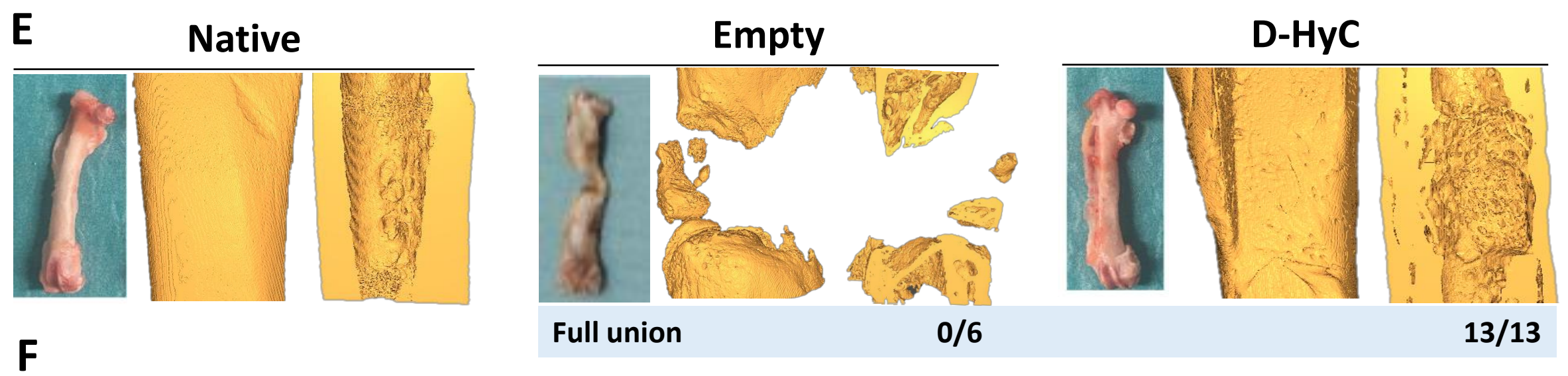
E
Native
Empty
D-HyC
Full union
0/6
13/13

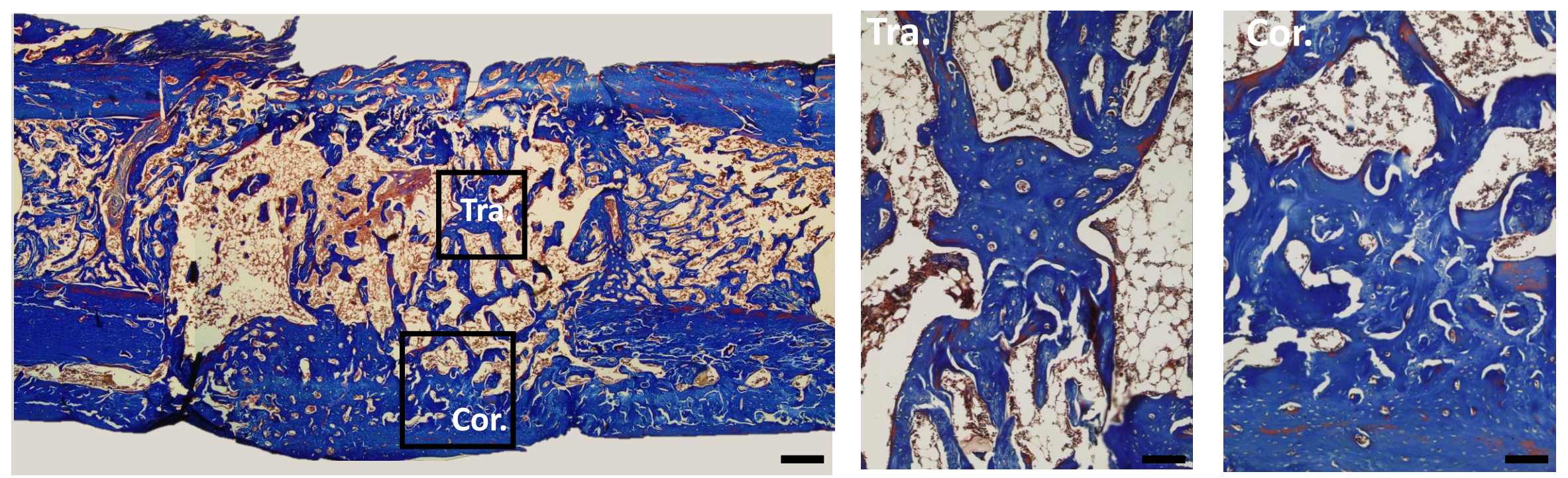
F
Tra.
Cor.
Tra.
Cor.

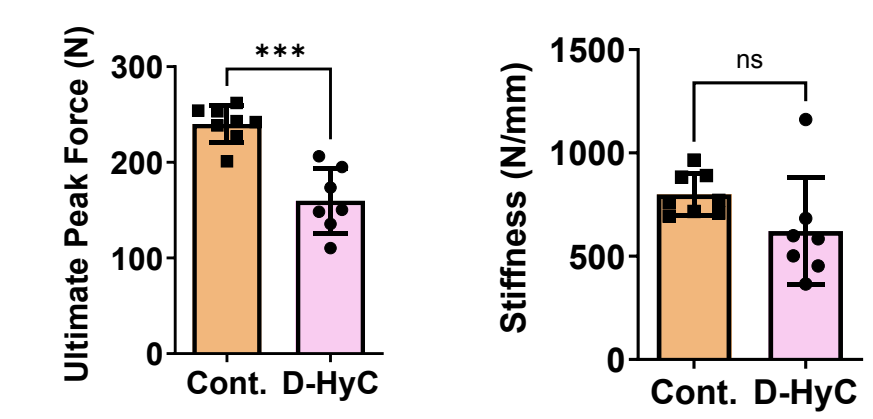
G
Ultimate Peak Force (N)
300
200
100
0
***
Cont.
D-HyC
Stiffness (N/mm)
1500
1000
500
0
ns
Cont.
D-HyC

Figure 6: Orthotopic immunocompetent rat critical-full sized femoral implantation of decellularized off-the-shelf MSOD-B cartilages confirms clinical potential. A. Experimental scheme of the assessment of bone regenerative potential of decellularized tissue engineered cartilages assessed in a critical full-sized femoral defect in immunocompetent rat. **B.** From left to right, macroscopic images of the empty critical full-sized defect and the defect fulfilled with a total of three engineered hypertrophic cartilage tissues. **C.** Micro-CT based representative 2D coronal (left) and sagittal (right) views from the middle of the defect after 4-, 6- and 12-weeks) for empty groups and regenerated femurs implanted with D-HyC. **D.** Quantification of micro-CT based bone volume (BV) in the defect (region of interest height = 4.5 mm) for empty groups and regenerated femurs implanted with D-HyC after 4-,6- and 12-weeks of implantation. The graphs represent mean + standard deviation (SD), ****$p \leq 0.0001$,, determined by Two-way ANOVA. **E.** From left to right, representative macroscopic image of an explanted regenerated femur at 12-weeks; representative 3D images of the entire defect area in both whole and cross-sectional view. **F.** From left to right, representative histological images of Masson Trichrome staining of explanted femurs completely regenerated after 12-weeks implantation with D-HyC; and a magnification of a region of interest of a cortical (cor.) and a trabecular (tra.) bone structure, Scale bar = 500 and 100 µm respectively. **G.** From left to right, Ultimate Peak Force (N) and total Stiffness (N/mm) for empty groups and regenerated femurs implanted with D-HyC after 12-weeks of implantation (n=8). The graphs represent mean + standard deviation (SD), ***$p \leq 0.001$,, determined by Two-way ANOVA.